



Transmission measurements and resonance parameter analysis for Mo-98 and Mo-100 [☆]



K.E Remley ^{a,*}, G. Leinweber ^a, D.P Barry ^a, R.C. Block ^a, M.J Rapp ^a, Y Danon ^b, R.M Bahrán ^c

^a Naval Nuclear Laboratory, P.O. Box 1072, Schenectady, NY 12301-1072, United States

^b Rensselaer Polytechnic Institute, 110 8th St., Troy, NY 12180, United States

^c Los Alamos National Laboratory, Los Alamos, NM 87545, United States

ARTICLE INFO

Article history:

Received 11 April 2018

Received in revised form 10 July 2018

Accepted 3 August 2018

Keywords:

Transmission

Resonance parameters

LINAC

Neutron cross sections

ABSTRACT

Molybdenum can exist in many nuclear reactor components, including fuel, cladding, or as a high yield fission product. As a result, accurate isotopic nuclear data for molybdenum are important for reactor simulation. To this end, high-resolution time-of-flight neutron transmission measurements on highly enriched isotopic metallic samples of Mo-98 and Mo-100 were performed and data were reduced to transmission in the resolved resonance region from 10 eV to 53 keV for Mo-98 and 10 eV to 26.5 keV for Mo-100. Measurements were taken with Li-6 glass transmission detectors at 31 m and 100 m flight paths. The Bayesian R-matrix code SAMMY 8.0 was used to shape-fit the data and to extract resonance parameters from the transmission spectra. The newly fitted resonance parameters were compared with those given in ENDF/B-VII.1. The results represent a refinement of those given in the current evaluation due to the improvement in the experimental resolution in these measurements. The comparison included analysis of level statistics. The resonance parameters for Mo-98 show many differences with the current evaluations. The results of the analysis indicated missing levels in Mo-98 starting at 10 keV, which implies an inability to resolve all resonances at higher energies. The resonance parameters for Mo-100 agree well with the current evaluation. Level statistics analysis indicates there are few missing levels up to 26.5 keV.

© 2018 Elsevier Ltd. All rights reserved.

1. Introduction

In nuclear energy applications, molybdenum has many uses, including presence in low-corrosion stainless steel and other alloys for reactor piping and fuel cladding. Molybdenum can also exist in nuclear reactors as a high-yield fission product. Further, it has been proposed that molybdenum can be alloyed with uranium as an advanced U-Mo nuclear fuel (Rest et al., 2009; Mason et al., 2011; Phillips et al., 2010). Because of these instances and uses of molybdenum, its nuclear properties are of great interest for reactor analysis.

Several prior measurements of molybdenum relevant to this work have taken place. Harvey et al. (1955) measured total cross sections for natural molybdenum up to 700 eV. Wynchank et al. (1968) measured total cross section in natural molybdenum from 6 eV to 250 keV while reporting resonance parameters to ~5 keV and extracting an estimate of the s-wave strength function. Shwe and Coté (1969) measured neutron transmission for enriched Mo-95 and Mo-97 samples as well as natural molybdenum up to 1.5 keV. From this measurement, they reported Γ_γ widths and strength functions for Mo-98 as well as an estimation of capture resonance integral for natural molybdenum. Chrien et al. (1976) measured and analyzed transmission measurements for Mo-98 to about 100 keV. In doing so, they reported resonance parameters up to 52.6 keV for Mo-98. It is also notable that they reported marked discrepancies from the work of Shwe and Coté (1969). Weigmann et al. (1979) measured transmission for enriched oxide samples of Mo-100, resulting in reported resonance parameters up to 26 keV. The more modern measurement of Wang et al. (2008) measured transmission for natural molybdenum, leading to reported resonance parameters up to 200 eV. A previous measurement on molybdenum was taken at the Rensselaer Polytechnic

[☆] This manuscript has been authored by Bechtel Marine Propulsion Corporation under Contract No. DE-NR000031 with the U.S. Department of Energy. The United States Government retains and the publisher, by accepting this article for publication, acknowledges that the United States Government retains a non-exclusive, paid-up, irrevocable, and world-wide license to publish, distribute, translate, duplicate, exhibit, and perform the published form of this manuscript, or allow others to do so, for United States Government purposes.

* Corresponding author.

E-mail address: kyle.remley@unnpp.gov (K.E Remley).

Institute (RPI) linear accelerator (LINAC) by [Leinweber et al. \(2010\)](#). This measurement featured transmission and capture measurements for natural molybdenum, which contributed to reported resonance parameters up to 2 keV.

The current work involved transmission measurements and resultant fitting and analysis of resonance parameters up to 53 keV for Mo-98 and 26.5 keV for Mo-100. This applicable energy range for measured transmission and resultant resonance parameters is greater than those discussed for many of the previous measurements, with the exception of the work of [Chrien et al. \(1976\)](#) and [Weigmann et al. \(1979\)](#). The relative dearth of experimental data found previously, including discrepancies between reported results, lends interest to the analysis of Mo-98 and Mo-100 resonance parameters discussed in this paper.

This measurement was run concurrently with those previously described in [Bahran et al. \(2015, 2013\)](#) and [Brown et al. \(2017\)](#). As discussed in the references ([Bahran et al., 2015, 2013](#); [Brown et al., 2017](#)), measurements of transmission between the energy range 1 keV and 620 keV were carried out for enriched samples of Mo-95, Mo-96, Mo-98, and Mo-100 at a nominal flight path of 100 m with the Mid-Energy Li-6 glass Neutron Detector Array (MELINDA) ([Bahran, 2013](#)). In addition, supplemental measurements of transmission in the range of 10 eV to 5 keV were carried out with the same enriched samples of molybdenum at a nominal flight path of 31 m with a different Li-6 glass detector system ([Barry, 2003](#)). Data from these measurements were reduced to transmission, and resonance parameters for Mo-98 and Mo-100 were extracted with the use of the Bayesian R-matrix resonance parameter code SAMMY ([Larson, 2008](#)). Where applicable, these new resonance parameters were compared with previous measurements. Further, a comparison of the new resonance parameters with the resonance parameters in ENDF/B-VII.1 ([Chadwick, 2011](#)) was carried out.

2. Experimental conditions

2.1. Experimental details

At the RPI Gaertner LINAC Center, an electron linear accelerator was used to bombard tantalum plates with electrons to produce neutrons. The incident electrons produced Bremsstrahlung radiation, which in turn produced neutrons via (γ, n) reactions. Neutrons were collimated into beams and bombarded samples along different beam flight paths. Measurements occurred at 31 m and 100 m flight paths. For both of these flight paths, sample placement was automated with a computer-controlled sample changer system. Each sample for a given measurement was cycled into and out of the neutron beam periodically to account for long-term machine fluctuations.

A separate set of neutron detectors operated on an adjacent beamline to the ones used in the measurements. The distance between the target and these neutron detectors was approximately 12 m. The purpose of these detectors was to measure fluctuations in the neutron beam intensity over the course of LINAC operation. These detectors are referred to as beam monitors, or simply mon-

itors. The data from these detectors were used to perform statistical checks of the measured data from the main detector. Further, for each measurement, one monitor was used as the neutron beam normalization standard.

The transmission data for Mo-98 and Mo-100 were collected over five total weeks. Three weeks of data collection occurred for measurements using the 31 m flight path, and two weeks of data collection occurred for measurements using the 100 m flight path. While the actual flight paths of these measurements varied slightly from these nominal values, it is convenient to refer to the measurements by these nominal flight path lengths.

For all measurements, the neutron-producing target was the C-shaped target ([Bahran, 2013](#); [Moretti, 1996](#)), the channel width for a time-of-flight measurement was 6.4 ns, and the repetition rate (pulses per second) of the beam was 400 pulses per second (pps). The remaining details of the experiment are given in [Table 1](#). These details include overlap filters, pulse widths, zero time (t_0), energy of the LINAC electron beam, average LINAC current, and flight path length. In [Table 1](#) the uncertainty in the flight path was derived from the mean free path of a neutron in the moderator of the C-shaped target. The nominal resolution, defined as the pulse width divided by flight path length, was ~ 0.4 ns/m for the 31 m flight path length measurements and ~ 0.1 ns/m for the 100 m flight path length measurements.

The zero time, t_0 , for the measured time-of-flight spectrum of each measurement was determined from a separate measurement and verified with U-238 transmission data. See Appendix A for details on the U-238 measurement. The uncertainty on each of these t_0 values was approximately 1 ns. This separate measurement determined the location of the count rate peak produced by the flash of gamma rays that accompanies each pulse of electrons from the LINAC. This peak is known as the gamma flash and coincides with the burst of neutrons from the target. For all cases except the first week of the 31 m measurements, the channel width for gamma flash measurements was 1.6 ns. For the first week of the 31 m measurements, the channel width for the gamma flash measurement was 6.4 ns. The channel width used was narrowed after the first week of 31 m measurements to allow for improved measurement of the centroid and spread of the gamma flash.

2.2. Sample information

For each measurement, a single sample of enriched Mo-98 and enriched Mo-100 was used. Each measurement subjected these to an incident neutron beam for the purpose of determining the uncollided fraction of neutrons penetrating the samples. The details of the Mo samples are given in [Table 2](#). The uncertainties in sample thicknesses were propagated from uncertainties in mass and diameter of the samples, where the diameter measurements were the primary source of sample thickness uncertainty. Information about the preparation of the samples is given in the thesis work of [Bahran \(2013\)](#).

From [Table 2](#), it is seen that two independent samples of both Mo-98 and Mo-100 were analyzed. In measurements, these were placed on top of each other and considered as composite samples

Table 1
Experimental Details for Mo-98 and Mo-100 transmission measurements.

Week	Overlap Filter	Pulse Width (ns)	t_0 (μ s)	LINAC Energy (MeV)	Average Current (μ A)	Flight Path Length (m)
1	Boron Carbide	14.0 \pm 0.1	2.340	56	15.5	31.89 \pm 0.01
2	Boron Carbide	12.0 \pm 0.1	5.229	47	11	31.94 \pm 0.01
3	Boron Carbide	14.0 \pm 0.1	5.560	50	20.5	31.94 \pm 0.01
1	Boron-10 pressed powder disk	10.5 \pm 0.1	6.070	50	13.6	100.14 \pm 0.01
2	Boron-10 pressed powder disk	11.0 \pm 0.1	6.412	51.5	22.8	100.14 \pm 0.01

Table 2

Sample Details. The rows labeled 'Composite' represent quantities for the composite sample, and the rows labeled '1' or '2' represent quantities for the individual samples that were stacked on each other to create the composite sample in measurements.

	Mo-98 Sample	Mo-100 Sample
Thickness 1 (mm)	2.08 ± 0.02	2.11 ± 0.02
Thickness 2 (mm)	4.83 ± 0.11	8.08 ± 0.03
Diameter 1 (mm)	50.69 ± 0.02	50.77 ± 0.01
Diameter 2 (mm)	50.85 ± 0.02	50.84 ± 0.03
Mass 1 (g)	35.9995	36.0225
Mass 2 (g)	90.6744	146.7077
Isotopic Mass 1 (g/mol)	97.8414 ± 0.0858	99.5460 ± 0.1909
Isotopic Mass 2 (g/mol)	97.8143 ± 0.0445	99.6801 ± 0.3504
Thickness 1 (atoms/b)	0.01098 ± 0.00003	0.01077 ± 0.00006
Thickness 2 (atoms/b)	0.02749 ± 0.00002	0.04367 ± 0.00012
Composite Thickness (atoms/b)	0.03847 ± 0.00004	0.0544 ± 0.0001
Composite Isotopic Mass (g/mol)	97.82	99.65
Composite Mo-92 Enrichment (atom %)	0.58	1.07
Composite Mo-94 Enrichment (atom %)	0.37	0.46
Composite Mo-95 Enrichment (atom %)	0.70	0.77
Composite Mo-96 Enrichment (atom %)	0.89	1.17
Composite Mo-97 Enrichment (atom %)	0.92	0.60
Composite Mo-98 Enrichment (atom %)	95.83	1.83
Composite Mo-100 Enrichment (atom %)	0.72	94.09

for Mo-98 and Mo-100. For the remainder of this paper, the composite samples are referred to simply as the samples, and the composite quantities were used in all subsequent analyses.

2.3. Transmission detectors

Transmission measurements were made using two separate Li-6 glass detectors. The 31 m measurements used the system previously implemented by Barry (2003). The 100 m measurements utilized the MELINDA detector system (Bahran, 2013). Thorough descriptions of these detector arrays are available in the references. The data from the 31 m measurements were analyzed from 10 eV to 3 keV, and the data from the 100 m measurements were analyzed from 3 keV to 53 keV for Mo-98 and 3 keV to 26.5 keV for Mo-100. The maximum dead time correction was 0.4% for the 31 m measurements and 1% for the 100 m measurements.

3. Data reduction

3.1. Transmission data

Data reduction to transmission includes a number of steps. These include correcting raw data for dead time, summing the counts from individual LINAC runs that correspond to the same sample and beam condition, normalizing data to monitors, determining the background correction, and computing the transmission. Transmission is defined as the ratio of the counting rate with a sample in the neutron beam to the counting rate with no sample in the neutron beam. This definition is given in Eq. (1):

$$T_i = \frac{C_{s,i} - k_s B_{s,i} - B_{0s}}{C_{o,i} - k_o B_{o,i} - B_{0o}} \quad (1)$$

In Eq. (1), T_i is the transmission, $C_{s,i}$ is the corresponding total count rate with the sample in the beam, $C_{o,i}$ is the total count rate for the open beam (no sample), $B_{s,i}$ is the time-dependent background with the sample in the beam, $B_{o,i}$ is the time-dependent background for the open beam, K_s is the sample time-dependent background normalization constant, k_o is the open beam time dependent background normalization constant, B_{0s} is the time-independent background for the sample, and B_{0o} is the time-independent background for the open beam. The subscript i indicates the i th energy (or time of flight) channel of the data. The transmission spectrum for a measurement is obtained by

applying Eq. (1) to every data point of the measurement in the energy region of interest. The measured transmission is directly linked to the total cross section of the sample material, and as such, the transmission can vary strongly with incident neutron energy, particularly over a resonance.

3.2. Neutron energy

In the experiment, neutron energy and neutron time of flight were assumed to be related using classical (i.e., non-relativistic) physical descriptions of kinetic energy of particles. Taking this assumption into account, the conversion between energy and time of flight grids for transmission data is given by

$$E_i = \left(\frac{KL}{t_i - t_0} \right)^2 \quad (2)$$

In Eq. (2) E_i is the energy at channel i , L is the flight path, t_0 is the zero time determined by the gamma flash measurement described in Section 2.1. t_i is the measured time of flight for channel i , and K is a physical constant. From Eq. (2) it is apparent that an important part of converting time to energy is correcting for the zero time. 'True' time of flight t_i is given by $t_i - t_0$.

3.3. Transmission background

Determination of background in a transmission experiment is a crucial part of the data reduction process. As seen in Eq. (1), the importance of background correction is related to its contribution to total count rate C_s , or $C_{o,i}$. This contribution is quantified in the signal-to-background ratio, which is defined at a single channel as R_i :

$$R_i = \frac{C_{o,i}}{k_o B_{o,i} + B_{0o}} - 1 \quad (3)$$

The signal-to-background ratios for the 31 m measurements are plotted in Fig. 1, and the signal-to-background ratios for the 100 m measurements are plotted in Fig. 2.

From Figs. 1 and 2 it is seen that the peak signal-to-background ratio is ~40 for the 31 m measurements and ~5 to 6 for the 100 m measurements. These plots demonstrate that, particularly at high energies, background contribution to total count rate is significant, and proper correction for background must be made. Differences in signal-to-background ratio are apparent between Weeks

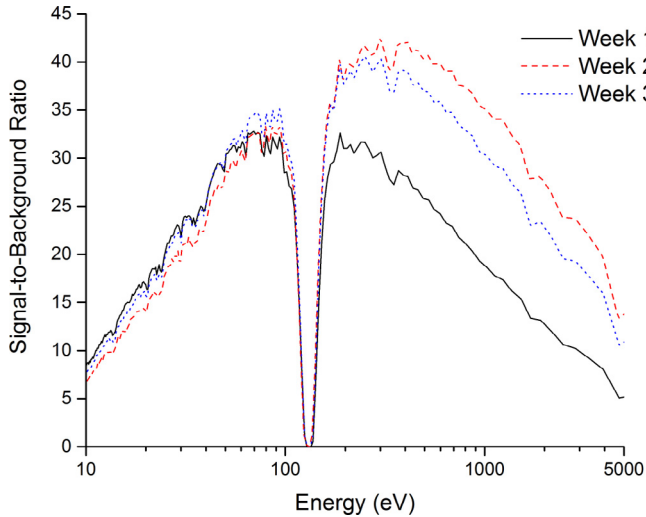


Fig. 1. Signal-to-background ratio for the 31 m measurements plotted over the range [10 eV, 5000 eV]. For all three weeks, the ratio goes to zero at 132 eV, the location of a cobalt black resonance that was used in all 31 m measurements.

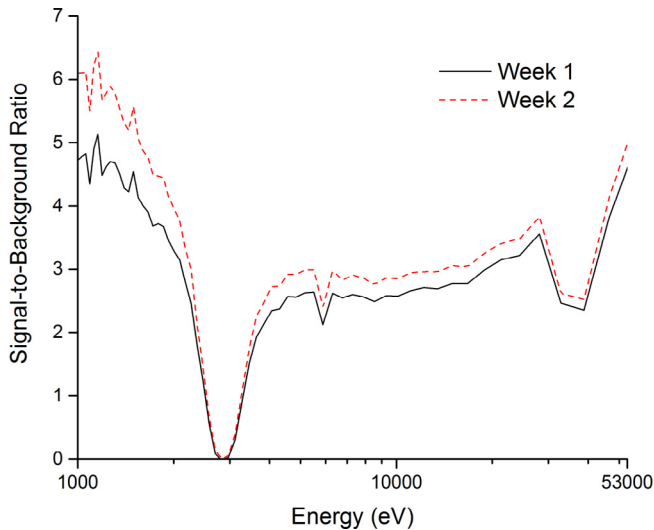


Fig. 2. The signal-to-background ratios for the 100 m measurements plotted over the range [1000 eV, 53000 eV]. For both weeks, the ratio goes to zero at 2850 eV, the location of a sodium black resonance that was used in all 100 m measurements.

(measurements) in Figs. 1 and 2. These differences can be attributed to changes in experimental parameters (e.g., those given in Table 1) and differences in the background between measurements.

In an experiment, background comes from multiple sources. There is a contribution from natural radiation from radioactive elements in the earth and cosmic rays. This background source is constant in time across multiple measurements. There is also a time-dependent contribution which consists of off-energy neutrons, gamma rays from neutron capture in the photonuclear target, and Bremsstrahlung x-rays. A portion of this is approximately constant in time. This constant portion was lumped together with background contributions from radioactive elements and cosmic rays. In Eq. (1), this component is B_0 .

Time-dependent background was determined through the method of black notches (Danon, 1993). In addition to measurements with a Mo sample in and out of the neutron beam, measurements were run with notch filters inserted into the beam. A notch filter is a material that has a strongly absorbing resonance at an energy of interest. When a notch filter is in the neutron beam,

Table 3

Notch filters used in the experiment. Each material has a saturated resonance where virtually all of the incident neutrons at the resonance energy are absorbed.

Notch Filter	Saturated Resonance Energy	Flight Path
W	18.8 eV	31 m
Co	132 eV	31 m
Mn	336 eV	31 m
Na	2850 eV	31 m & 100 m
Al	35 keV	100 m
S	106 keV	100 m
Li	260 keV	100 m

any counts that are observed at that energy are attributed to background. Several measurements were run with different notch filters, and the resultant observed count rates at the notch filter energies were placed on the time-of-flight grid and used in a non-linear least-squares fit to determine a functional form of the time-dependent background. The fitted function for the background was then used for the time-of-flight interval bounded by the times-of-flight corresponding to the minimum and maximum notch filter energies. The notch filters used for the 31 m and 100 m measurements are given in Table 3.

The assumed functional forms of the time-dependent background shapes are given for the 31 m measurements in Eq. (4) and for the 100 m measurements in Eq. (5):

$$B(t) = at^{-b} \quad (4)$$

$$B(t) = ce^{-dt} + fe^{-gt} \quad (5)$$

In Eq. (4), the fitted parameters are $\{a, b\}$, and in Eq. (5), the fitted parameters are $\{c, d, f, g\}$. In Eqs. (4) and (5), the independent variable t is in time-of-flight; that is, $t = t' - t_0$, where t' , t_0 are from Eq. (2).

While this method is effective in obtaining a shape of the background, the presence of the notch filters themselves attenuates some of the background. To overcome this, the time-dependent background was normalized to a fixed notch. Unlike the notches only placed into the neutron beam to determine background, the fixed notch was always present during measurements. In fact, the presence of the fixed notch is noticeable in Figs. 1 and 2: the energy at which the signal-to-background ratio goes to zero is the energy of the black resonance of the fixed notch. The normalization is given by Eq. (6):

$$k = \frac{B_{fixed} - B_0}{B(t)} \quad (6)$$

In Eq. (6), B_{fixed} is the observed count rate at the fixed notch energy, and k is the normalization constant. As indicated by Eq. (1), a normalization constant was found for each sample and open beam time-dependent background functions.

The fixed notch used in the 31 m measurements was Co with a resonance energy of 132 eV. For the 100 m measurements, the fixed notch was Na with a resonance energy of 2850 eV. While it is not ideal to use the fixed notch in the determination of the background shape as was done for the 100 m measurements, this was necessary to extend the applicable energy range of the time dependent background function over the entire resolved resonance region for Mo-98 and Mo-100.

4. Results

4.1. Resonance parameters

The Bayesian multi-level R-matrix code SAMMY 8.0 (Larson, 2008) was used to fit resonance parameters to the reduced

Table 4
Mo-98 resonance parameters.

$J\pi$		l		$E(\text{eV})$			Γ_γ (meV)	Γ_n (meV)		
ENDF	NNL/RPI	ENDF	NNL/RPI	ENDF	NNL/RPI	Unc.		ENDF	NNL/RPI	Unc.
0.5	0.5	0	0	-980	-980	0	85	4710	4710	0
-1.5	-1.5	1	1	12.1	12.07	0.01	120	0.029	0.035	0.005
-1.5	-1.5	1	1	402	401.56	0.02	120	1.62	1.46	0.05
-0.5	-0.5	1	1	430	429.16	0.01	123	73.4	92	3
0.5	0.5	0	0	468	467.23	0.02	96	759	763	8
-0.5	-0.5	1	1	613	612.18	0.01	143	65.8	60	2
-1.5	-1.5	1	1	819	817.77	0.02	103	68	68	2
-1.5	-1.5	1	1	1124	1122.5	0.1	120	10.4	9.7	0.4
0.5	0.5	0	0	1529	1526.5	0.1	71.8	1280	1350	20
-1.5	-1.5	1	1	1927	1920.8	0.3	120	11	9.9	0.6
-0.5	-0.5	1	1	2026	2018.1	0.9	120	2.55	4.1	0.4
-0.5	-1.5	1	1	2182	2177.2	0.1	128	170	169	8
-0.5	-1.5	1	1	2465	2462.0	0.1	134	93	78	4
0.5	0.5	0	0	2553	2548.9	0.1	70	888	1170	20
-1.5	-1.5	1	1	2617	2612.9	0.3	120	24.7	27	2
-0.5	-1.5	1	1	2951	2946.3	0.4	120	57.8	26	2
-0.5	-1.5	1	1	3269	3264.0	0.4	120	47.4	24	2
0.5	0.5	0	0	3302	3296.6	0.1	65	1480	1760	40
-1.5	-1.5	1	1	3804	3797.1	0.1	106	186	157	8
-1.5	-1.5	1	1	4023	4016.0	0.1	164	86.2	114	5
0.5	0.5	0	0	4486	4478.4	0.1	84	428	540	20
-1.5	-1.5	1	1	4579	4570.4	0.1	138	165	182	8
-1.5	-1.5	1	1	4858	4848.9	0.1	126	206	240	10
-1.5	-1.5	1	1	5282	5272.8	0.1	75	584	570	20
-0.5	-0.5	1	1	5430	5419.3	0.6	120	49.4	56	5
0.5	0.5	0	0	5610	5600.8	0.1	86	1945	3320	40
-0.5	-0.5	1	1	5651	5640.8	0.1	146	641	610	30
-0.5	-0.5	1	1	5931	5931.0	0.2	150	1161	1160	60
0.5	0.5	0	0	6179	6183.3	0.1	44	6600	7290	70
-0.5	-0.5	1	1	6197	6207	1	120	55.6	29	3
-0.5	-0.5	1	1	6690	6679.2	0.4	105	178	130	10
-1.5	-1.5	1	1	6833	6820.9	0.1	87.4	442	400	20
-0.5	-0.5	1	1	7111	7104.8	1	120	36.5	44	4
-0.5	-0.5	1	1	7196	7185.0	0.6	91.4	184	115	9
0.5	0.5	0	0	7515	7503.4	0.1	71	4035	5280	70
-0.5	-0.5	1	1	7613	7598.6	0.2	137	509	630	30
-1.5	-1.5	1	1	7981	7967.4	0.2	94	453	400	20
-1.5	-1.5	1	1	8580	8565.7	0.1	103	1257	1660	50
-0.5	-0.5	1	1	8616	8603	1	120	67	69	6
-1.5	-1.5	1	1	8840	8825.1	0.2	117	598	710	30
0.5	0.5	0	0	9045	9037.4	0.3	125	35,830	47,700	300
-0.5	-0.5	1	1	9385	9359	2	51	210	55	5
-0.5	-0.5	1	1	9450	9453	3	120	15.8	13	1
-1.5	-1.5	1	1	9686	9670.1	0.2	66	764	1210	50
-0.5	-0.5	1	1	9749	9732.6	0.4	115	214	570	30
-0.5	-0.5	1	1	10,053	10035.0	0.4	102	391	590	40
0.5	0.5	0	0	10,600	10586.4	0.2	65.4	12,030	15,300	200
-1.5	-1.5	1	1	10,900	10880.6	0.5	86.6	339	360	20
-0.5	-0.5	1	1	11,310	11290.9	0.7	58	319	410	30
-1.5	-1.5	1	1	11,361	11342.7	0.2	98	1540	1900	70
0.5	-0.5	0	1	11,598	11578.1	0.2	79	1936	3000	100
-1.5	-1.5	1	1	11,703	11688.4	0.2	131	3460	4700	100
-1.5	-1.5	1	1	12,020	11997.7	0.2	81	2846	4800	100
-1.5	-1.5	1	1	12,100	12080.4	0.4	95	571	700	40
-0.5	-0.5	1	1	12,856	12,832	1	120	260	390	30
-0.5	-0.5	1	1	13,005	13,020	2	120	260	110	10
-1.5	-1.5	1	1	13,160	13,137	1	93.5	407	510	30
-1.5	-1.5	1	1	13,420	13411.6	0.3	97.3	1042	1310	70
-0.5	-0.5	1	1	13,943	13916.5	0.6	120	120	860	60
-0.5	-0.5	1	1	14,030	14,044	3	120	92	130	10
-0.5	-0.5	1	1	14,080	14,102	3	120	434	84	8
-1.5	-1.5	1	1	14,630	14600.4	0.6	84.6	272	630	40
-1.5	-1.5	1	1	14,785	14759.5	0.3	90	2550	4600	100
0.5	0.5	0	0	14,825	14793.2	0.3	86	3770	4000	100
-1.5	-1.5	1	1	15,250	15223.9	0.4	91	765	1020	50
-0.5	-0.5	1	1	15,330	15,296	2	120	291	360	30
-0.5	-0.5	1	1	15,780	15,764	1	120	215	600	50
0.5	-0.5	0	1	15,940	15918.4	0.5	86	1500	2100	100
-1.5	-1.5	1	1	16,238	16202.8	0.8	95	382	530	40
0.5	0.5	0	0	16,500	16469.3	0.5	67	2440	2500	100
-1.5	-1.5	1	1	16,740	16708.7	0.6	89	387	1240	80
-0.5	-0.5	1	1	16,995	16964.1	0.5	125	3250	3700	200
-1.5	-1.5	1	1	17,380	17,347	1	120	275	440	30

(continued on next page)

Table 4 (continued)

$J\pi$		l		$E(\text{eV})$			$\Gamma_\gamma (\text{meV})$	$\Gamma_n (\text{meV})$		
ENDF	NNL/RPI	ENDF	NNL/RPI	ENDF	NNL/RPI	Unc.		ENDF	NNL/RPI	Unc.
-0.5	-0.5	1	1	17,640	17615.6	0.5	123	3650	4100	200
-1.5	-1.5	1	1	17,745	17,708	2	120	174	210	20
-0.5	-0.5	1	1	18,045	18,043	5	120	43.6	37	4
-1.5	-1.5	1	1	18,335	18302.7	0.6	92	473	1390	80
-1.5	-1.5	1	1	18,580	18,533	4	120	82.8	64	6
-1.5	-1.5	1	1	19,060	19,020	1	120	618	560	40
0.5	0.5	0	0	19,285	19261.9	0.4	98	4580	5700	200
-1.5	-1.5	1	1	19,625	19595.1	0.4	124	4690	6700	200
-1.5	-1.5	1	1	19,745	19,761	4	120	200	120	10
-0.5	-0.5	1	1	19,910	19,933	4	120	193	180	20
-1.5	-1.5	1	1	20,030	19,992	1	123	424	820	60
-0.5	-0.5	1	1	20,255	20,217	1	130	1280	3500	200
-0.5	-0.5	1	1	20,865	20,854	4	120	360	210	20
-1.5	-1.5	1	1	21,170	21,185	5	120	95	83	8
-0.5	-0.5	1	1	21,395	21,408	5	120	109	100	10
-0.5	-0.5	1	1	21,530	21,538	5	120	72	67	7
-1.5	-1.5	1	1	21,675	21636.8	0.6	120	180	2900	100
-1.5	-1.5	1	1	21,950	21913.0	0.8	197	1553	1800	100
-1.5	-1.5	1	1	22,070	22031.9	0.6	92	2150	4200	200
-1.5	-1.5	1	1	22,570	22528.4	0.9	102	825	1500	100
-1.5	-1.5	1	1	22,980	22,934	1	117	832	1500	100
-0.5	-0.5	1	1	23,180	23,194	6	120	82.8	82	8
-1.5	-1.5	1	1	23,545	23499.4	0.5	154	5820	11,700	300
-0.5	-0.5	1	1	23,680	23,640	1	158	1075	2400	200
-1.5	-1.5	1	1	23,945	23,941	5	120	223	110	10
-0.5	-0.5	1	1	24,370	24,320	1	97	1870	3400	200
-0.5	-1.5	1	1	24,480	24,524	1	120	280	7700	200
-1.5	-0.5	1	1	24,580	24,636	5	126	3834	240	20
-0.5	-0.5	1	1	24,920	24,873	1	80	945	2300	200
-1.5	-1.5	1	1	25,540	25,486	1	98	2870	6400	300
-1.5	-1.5	1	1	25,610	25,567	1	108	800	2000	100
-1.5	-1.5	1	1	26,080	26017.0	0.7	160	1740	4900	200
-1.5	-1.5	1	1	26,190	26,152	2	120	480	690	60
-1.5	-1.5	1	1	26,930	26,884	2	120	492	840	70
-1.5	-1.5	1	1	27,150	27091.2	0.7	137	2550	5900	200
-0.5	-0.5	1	1	27,680	27,625	2	157	1163	2900	200
-1.5	-1.5	1	1	27,860	27,806	1	138	1500	3400	200
-1.5	-1.5	1	1	27,960	27,905	3	120	1130	600	50
-0.5		1		28,330			120	360		
0.5	-0.5	0	1	28,700	28656.0	0.7	162	10,150	15,600	400
-1.5		1		28,920			120	157		
-0.5	-0.5	1	1	29,090	29,047	3	120	600	1700	100
-0.5	-0.5	1	1	29,430	29,415	2	133	1885	2900	200
-0.5	-0.5	1	1	29,720	29,672	2	120	680	3300	200
-1.5	-1.5	1	1	29,850	29,786	2	155	776	1800	100
-1.5		1		30,170			120	323		
-0.5		1		30,460			120	137		
0.5	-0.5	0	1	30,610	30,624	1	100	43,900	50,000	1000
-1.5	0.5	1	0	30,680	30,683	1	214	4115	31,800	900
-1.5	-0.5	1	1	31,200	31,153	2	190	1763	5200	300
-0.5	0.5	1	0	31,540	31,459	1	120	3190	5800	300
-0.5	-0.5	1	1	32,040	31,982	1	120	5180	11,300	500
-0.5	-0.5	1	1	32,160	32,092	1	120	6450	10,700	500
-0.5	-0.5	1	1	32,470	32,406	1	120	4000	9400	500
	-0.5		1		33,278	8	85		580	60
	0.5		0		33,317	3	85		3700	300
-0.5	-0.5	1	1	33,430	33,395	2	120	5100	11,500	600
	-0.5		1		33,529	3	118		5600	400
-0.5	-0.5	1	1	33,810	33,749	2	120	3120	8500	600
-0.5	-0.5	1	1	33,980	33,920	2	120	7550	14,300	900
0.5	-0.5	0	1	36,160	36,086	2	85	21,600	39,000	2000
0.5	-0.5	0	1	36,920	36,845	2	85	13,400	25,000	1000
-0.5	-0.5	1	1	37,200	37,109	3	120	3470	6800	500
0.5	-0.5	0	1	37,770	37,704	2	85	17,100	28,000	1000
	-0.5		1		38,190	10	85		300	30
	-0.5		1		38,220	10	85		280	30
0.5	-1.5	0	1	38,350	38,279	1	85	31,700	29,300	700
0.5	-1.5	0	1	38,800	38,722	1	85	22,600	22,200	600
	-0.5		1		39,472	4	85		3800	300
-0.5	-0.5	1	1	39,590	39,531	3	120	5560	6200	400
-0.5	-0.5	1	1	40,110	40,017	2	120	3800	9500	500
-0.5	-0.5	1	1	40,860	40,789	2	120	4040	10,800	600
	-0.5		1		41,210	10	85		230	20
-0.5	-0.5	1	1	41,440	41,365	3	120	5080	12,500	800

Table 4 (continued)

$J\pi$		l		$E(\text{eV})$			Γ_γ (meV)	Γ_n (meV)		
ENDF	NNL/RPI	ENDF	NNL/RPI	ENDF	NNL/RPI	Unc.		ENDF	NNL/RPI	Unc.
-0.5	-0.5	1	1	41,820	41,728	3	120	6530	10,700	700
-0.5	0.5	1	0	43,080	42,986	2	120	11,200	22,600	800
-0.5		1		43,120			120	2280		
-0.5	-0.5	1	1	44,120	44,042	4	120	2310	4800	400
-0.5	-0.5	1	1	44,240	44,175	3	120	3360	11,200	600
-0.5	0.5	1	0	44,490	44,403	2	120	10,700	20,400	800
0.5	-0.5	0	1	44,860	44,790	2	85	15,200	30,100	900
0.5	0.5	0	0	45,280	45,163	1	85	61,000	92,000	1000
0.5	-0.5	0	1	45,820	45,750	2	85	27,800	36,000	1000
-0.5		1		45,980			120	3210		
0.5	-0.5	0	1	46,110	46,026	2	85	15,400	21,300	900
-0.5	-0.5	1	1	47,300	47,223	6	120	3910	3400	300
0.5	0.5	0	0	48,600	48,479	1	85	28,800	49,000	1000
-0.5	-0.5	1	1	49,440	49,330	10	120	9100	21,600	900
0.5	-0.5	0	1	49,970	49,338	2	85	20,300	31,000	1000
-0.5	-0.5	1	1	52,260	49,886	2	120	9130	21,600	900
0.5	-0.5	0	1	52,790	52,165	3	85	22,000	45,000	1000

transmission data. The analysis employed several features of the SAMMY code, including the experimental resolution, Doppler broadening, and propagated uncertainty parameters. The effective temperature used in the analysis for Doppler broadening was 318 K. The function modeling the experimental resolution (the ‘resolution function’) used in the analysis was the ‘Oak Ridge Resolution Function’ described in the SAMMY manual (Larson, 2008). The choices for the parameters and uncertainties for this resolution function are described in detail in the thesis work of Bahran (2013). In addition, the choice for resolution function was validated by performing transmission measurements on U-238. Data from these measurements were plotted against fits using resonance parameters for U-238 from ENDF/B-VII.1, the details of which are given in Appendix A. The sources of experimental uncertainty used for propagation in SAMMY through its Propagated Uncertainty Parameter (PUP) capability were experimental resolution function, transmission normalization, transmission background, flight path length, t_0 , burst width, sample thickness, and effective temperature. The quantification and inclusion of these uncertainty sources follows the methods of previous analyses (Bahran, 2013; Epping et al., 2017; Leinweber et al., 2014; Block et al., 2017).

Transmission data from both the 31 m measurements and the 100 m measurements were used to determine resonance parameters. The data from the 31 m measurements were used to determine resonance parameters from 10 eV to 3 keV, and the data from the 100 m measurements were used to determine resonance parameters from 3 keV to 53 keV for Mo-98 and 3 keV to 26.5 keV for Mo-100. The reason for this choice is that the background measurements used in reduction of the 31 m data were optimized for the energy range 10 eV to 3 keV and the background measurements used in reduction of the 100 m data were optimized for the energy range 3 keV to 53 keV. In the Mo-100 fitting process, two resonances were exceptions to this rule. The fitted resonance parameters for the resonance at 1766 eV were taken from the 100 m data, and the resonance parameters for the resonance at 3605 eV were taken from the 31 m data. The reason for these exceptions was that the fits agreed better with the experimental data and the fitted parameters were closer to the values given in ENDF/B-VII.1. Further discussion of these two exceptions is found in Appendix B.

In the fitting process, only the neutron widths, Γ_n , were allowed to vary while radiation widths Γ_γ were held at ENDF/B-VII.1 values. This is because there were no capture measurements were carried out that could give insight into the radiation widths.

The newly fitted resonance parameters for Mo-98 are listed in Table 4. The newly fitted resonance parameters for Mo-100 are listed in Table 5. Each of these tables provides a comparison to the resonance parameters given in ENDF/B-VII.1, (Chadwick, 2011) where columns labeled ‘ENDF’ represent those resonance parameters, and columns labeled ‘NNL/RPI’ represent the newly fitted resonance parameters. In Tables 4 and 5, the resonances for each isotope are given in increasing energy order. Missing entries indicate that a resonance was newly added (if the missing entry is in the ENDF columns) or that a resonance was removed (if the missing energy is in the NNL/RPI columns). All given uncertainties are for the newly fitted parameters. The uncertainties represent the results from the Bayesian fitting process. The values of Γ_γ are given in a single column rather than for ‘ENDF’ or ‘NNL/RPI’ since they were not varied in the fitting process. For resonances that were added in analysis, the value of Γ_γ presented in the tables was selected from a neighboring average. Further, uncertainty for Γ_γ values are not reported since they were not fitted in the analysis.

To give a graphical view of the results, fits with new resonance parameters as well as fits with the resonance parameters from ENDF/B-VII.1 are given in Fig. 3 for Mo-98 and Fig. 4 for Mo100.

Fig. 3 and Table 4 show sharp contrast between the newly fitted parameters resulting from the Mo-98 measurement and those from the most recent evaluation. Particularly at high energies, the newly fitted resonance parameters (and resultant transmission fit) differ quite significantly from the resonance parameters of ENDF/B-VII.1. In the fitting process, the assignment of several s-wave resonances were changed to p-wave resonances to improve the observed fits. ENDF/B-VII.1 features 30s-wave resonance parameters for Mo-98, and NNL/RPI featured 21s-wave resonance parameters for Mo-98. In addition to changing many s-waves to p-waves, Table 4 shows many added and removed resonances in the newly fitted resonance parameters compared to those in the most recent evaluation. Fig. 3 shows the effects of some of these changes.

Unlike the case for Mo-98, Fig. 4 and Table 5 show that the new measurement for Mo-100 resulted in resonance parameters that were only slightly different from the previous evaluation; the main effect of the new data is a recommended shift of the resonance energies – an example of this shift is given in Fig. 4. The energy shift was confirmed by a simultaneous measurement of uranium resonances – see Appendix A. In addition, a few new resonances were added to improve the fit.

Table 5
Mo-100 Resonance Parameters.

$J\pi$		l		E (eV)			Γ_γ (meV)	Γ_n (meV)		
ENDF	NNL/RPI	ENDF	NNL/RPI	ENDF	NNL/RPI	Unc.		ENDF	NNL/RPI	Unc.
0.5	0.5	0	0	-172	-172	0	64	171.5	171.5	0
-1.5	-1.5	1	1	97.2	97.3	0.1	80	0.18	0.20	0.01
0.5	0.5	0	0	363.7	363.80	0.01	70	640	590	10
-0.5	-0.5	1	1	507.4	506.90	0.01	80	4.4	5.1	0.3
-0.5	-0.5	1	1	536.1	535.50	0.02	80	4.2	5.6	0.4
-0.5	-0.5	1	1	787.4	786.20	0.03	80	5.8	6.9	0.4
-1.5	-1.5	1	1	1070.7	1069.20	0.02	104	65	90	5
-1.5	-1.5	1	1	1263	1260.80	0.03	89	50	63	4
0.5	0.5	0	0	1407.4	1404.20	0.04	46	116	120	4
-1.5	-1.5	1	1	1700.4	1697.00	0.06	69	180	210	20
-0.5	-0.5	1	1	1769.5	1766.30	0.06	89	21	20	1
0.5	0.5	0	0	1941.1	1937.50	0.05	56	1010	1060	20
-0.5	-0.5	1	1	2066	2063.0	0.5	80	6.5	9	1
-1.5	-1.5	1	1	2425	2420.7	0.1	56	260	330	20
0.5	0.5	0	0	2636	2630.5	0.09	65	410	500	20
-1.5	-1.5	1	1	2671	2667.0	0.7	66	6	6.7	0.9
-1.5	-1.5	1	1	2962	2956.0	0.3	80	25.8	21	2
0.5	0.5	0	0	3015	3007.0	0.6	50	1950	2000	100
-0.5	-0.5	1	1	3078	3079.0	0.4	110	101	110	20
-1.5	-1.5	1	1	3269	3266.2	0.2	104	69	63	5
-1.5	-1.5	1	1	3547	3539.6	0.2	80	35	34	2
-0.5	0.5	1	0	3557	3549.3	0.1	73	99	122	7
-1.5	-1.5	1	1	3613	3605.4	0.3	80	61	61	6
-1.5	-1.5	1	1	4165	4159.0	0.7	99	8	7	1
0.5	-1.5	0	1	4521	4511.6	0.1	81	870	520	30
-1.5	-1.5	1	1	4559	4550.5	0.1	89	87.5	77	5
0.5	0.5	0	0	4745	4735.5	0.1	68	195	155	8
-0.5	-0.5	1	1	4788	4787	1	97	15	11	2
0.5	0.5	0	0	5168	5157.3	0.1	70	5480	5190	70
-0.5	-0.5	1	1	5250	5240.3	0.5	80	63	42	5
	-0.5		1		5601.3	0.5	85		68	5
0.5	0.5	0	0	5636	5625.2	0.1	73	7700	7100	90
-0.5	-0.5	1	1	5732	5720	1	80	19.3	14	3
-0.5	-0.5	1	1	6005	5995.2	0.1	61	660	500	30
-1.5	-1.5	1	1	6126	6113.2	0.1	75	175	152	9
-1.5	-1.5	1	1	6393	6380.4	0.1	80	275	220	10
-1.5	-1.5	1	1	6690	6677.9	0.2	80	140	137	9
-1.5	-1.5	1	1	7095	7081.3	0.2	79	138	190	10
0.5	0.5	0	0	7273	7258.3	0.1	70	4680	4100	70
-0.5	-0.5	1	1	7628	7628.6	0.3	80	162	260	20
-0.5	-0.5	1	1	7642	7650.1	0.3	80	269	360	40
0.5	0.5	0	0	7673	7661.2	0.3	51	6000	5000	100
-0.5	-0.5	1	1	7703	7689.1	0.5	64	1000	190	20
-1.5	-1.5	1	1	7940	7922.8	0.6	62	105	60	7
-1.5	-1.5	1	1	8215	8198.9	0.2	89	117	340	20
0.5	0.5	0	0	8440	8423.7	0.3	59	470	390	30
0.5	0.5	0	0	8800	8781.6	0.2	62	1030	850	40
-1.5	-1.5	1	1	9008	8988.3	0.2	78	550	620	40
-0.5	-0.5	1	1	9253	9247	2	80	32	45	7
-1.5	-1.5	1	1	9610	9591.1	0.3	75	205	210	10
0.5	0.5	0	0	9658	9639.2	0.2	67	2900	2700	80
-0.5	-0.5	1	1	9833	9816.1	0.6	73	210	190	20
-0.5	-0.5	1	1	9943	9914	2	80	68	70	10
-1.5	-1.5	1	1	10,210	10191.0	0.2	59	825	760	50
-1.5	-1.5	1	1	10,420	10,400	1	57	138	62	9
-0.5	-0.5	1	1	10,648	10630.0	0.3	61	670	720	50
-1.5	-1.5	1	1	10,940	10919.0	0.5	70	165	190	20
-1.5	-1.5	1	1	11,055	11035.0	0.8	92	103	110	10
0.5	0.5	0	0	11,398	11372.0	0.5	112	778	460	40
-0.5	-0.5	1	1	11,593	11570.0	0.5	76	335	450	30
-0.5	-0.5	1	1	11,728	11709.0	0.2	75	2900	2500	100
0.5	0.5	0	0	11,985	11958.0	0.2	68	12,000	10,900	200
-0.5	-0.5	1	1	12,152	12,130	2	80	377	140	20
-0.5	-0.5	1	1	12,463	12438.0	0.3	83	3200	2600	100
-0.5	-0.5	1	1	12,568	12,540	2	92	220	150	20
-0.5	-0.5	1	1	12,642	12,640	2	38	190	150	20
-0.5	-0.5	1	1	12,688	12663.0	0.5	94	580	610	50
-1.5	-1.5	1	1	12,725	12700.0	0.8	79	165	180	20
-0.5	-0.5	1	1	13,060	13039.0	0.7	68	670	540	50
-1.5	-1.5	1	1	13,429	13,406	1	80	91	120	20
-1.5	-1.5	1	1	13,545	13518.0	0.3	80	2900	2500	100
-0.5	-0.5	1	1	13,941	13916.0	0.8	73	570	410	40
0.5	0.5	0	0	13,997	13972.0	0.3	70	2440	1850	90

Table 5 (continued)

$J\pi$		l		E (eV)			Γ_γ (meV)	Γ_n (meV)		
ENDF	NNL/RPI	ENDF	NNL/RPI	ENDF	NNL/RPI	Unc.		ENDF	NNL/RPI	Unc.
-0.5	-0.5	1	1	14,203	14178.0	0.5	58	990	1040	70
0.5	0.5	0	0	14,748	14720.0	0.4	55	2160	1480	80
-1.5	-1.5	1	1	15,261	15228.0	0.9	73	158	250	20
-1.5	-1.5	1	1	15,346	15318.0	0.3	80	2375	2600	100
-0.5	-0.5	1	1	15,581	15553.0	0.6	80	320	1330	70
0.5	0.5	0	0	15,635	15604.0	0.3	60	22,200	20,300	300
-1.5	-1.5	1	1	15,757	15731.0	0.9	89	368	370	40
-1.5	-1.5	1	1	15,898	15867.0	0.4	60	2500	2600	100
-1.5	-1.5	1	1	16,017	15988.0	0.8	80	355	420	40
-0.5	-0.5	1	1	16,470	16441.0	0.4	91	5800	5900	200
0.5	0.5	0	0	16,666	16631.0	0.3	78	14,300	11,900	200
-1.5	-1.5	1	1	16,800	16,772	2	87	590	510	80
0.5	0.5	0	0	16,925	16893.0	0.6	80	1660	1300	100
-1.5	-1.5	1	1	17,132	17103.0	0.8	100	450	590	50
-1.5	-1.5	1	1	17,525	17,503	1	97	225	340	30
0.5	0.5	0	0	17,696	17660.0	0.4	49	26,200	23,200	400
-1.5	-1.5	1	1	18,009	17,976	2	80	560	200	30
	0.5		0		18229.0	0.4	82		3900	200
-1.5	-1.5	1	1	18,645	18,614	1	80	350	320	40
-1.5	-1.5	1	1	19,064	19,040	3	80	82	130	20
0.5	0.5	0	0	19,355	19320.0	0.5	62	2650	2900	100
-1.5	-1.5	1	1	19,663	19,639	2	108	285	320	40
-1.5	-1.5	1	1	19,895	19854.0	0.5	133	2200	2800	100
0.5	0.5	0	0	20,094	20056.0	0.4	84	13,500	10,600	300
-1.5	-1.5	1	1	20,147	20,100	3	80	86	110	20
-0.5	-0.5	1	1	20,563	20,550	5	80	36	36	7
-0.5	-0.5	1	1	20,672	20,680	5	80	62	82	20
0.5	0.5	0	0	20,735	20698.0	0.4	50	10,400	8200	200
-1.5	-1.5	1	1	20,877	20847.0	0.9	87	1245	1040	90
-1.5	-1.5	1	1	21,213	21175.0	0.6	102	3200	2600	200
-1.5	-1.5	1	1	21,571	21535.0	0.5	130	6500	6500	200
-1.5	-1.5	1	1	21,810	21771.0	0.9	110	1410	1200	100
0.5	0.5	0	0	22,174	22124.0	0.6	76	7300	5100	200
-1.5	-1.5	1	1	22,232	22,190	2	80	377	310	40
0.5	0.5	0	0	22,400	22356.0	0.5	81	7600	7300	200
0.5	0.5	0	0	22,822	22783.0	0.5	61	13,700	12,300	300
-1.5	-1.5	1	1	22,960	22,921	1	116	2900	2700	400
	-0.5		1		22,930	5	81		460	90
-1.5	-1.5	1	1	23,153	23109.0	0.7	77	2000	2000	100
0.5	0.5	0	0	23,403	23350.0	0.7	49	6000	4500	200
-0.5	-0.5	1	1	23,521	23,470	4	80	276	260	40
-0.5	-0.5	1	1	23,594	23,640	6	80	72	67	10
0.5	0.5	0	0	23,880	23815.0	0.5	63	18,200	16,400	400
-0.5	-0.5	1	1	23,914	23,980	6	80	56	70	10
-1.5	-1.5	1	1	24,235	24,180	4	80	123	140	30
-0.5	-0.5	1	1	24,341	24,289	1	46	2900	2900	200
-1.5	-1.5	1	1	24,438	24390.0	0.9	110	2200	2000	100
0.5	0.5	0	0	24,590	24541.0	0.5	94	18,500	15,500	400
-1.5	-1.5	1	1	24,982	24,933	1	71	1950	1900	100
-1.5	-1.5	1	1	25,222	25,180	3	86	470	450	60
-1.5	-1.5	1	1	25,740	25694.0	0.8	90	4250	4200	200
0.5	0.5	0	0	25,827	25776.0	0.6	42	8700	8300	300
-1.5	-1.5	1	1	25,975	25929.0	0.8	102	5200	4700	200
-1.5	-1.5	1	1	26,165	26,104	1	72	700	1200	100

4.2. Nuclear level statistics

To further analyze the impact of the new measurements, analysis of level statistics was carried out for both Mo-98 and Mo-100. Of particular interest were level densities, strength functions, and distributions of neutron widths.

4.2.1. Level density

The average level spacings, D_0 , were computed for the s-wave resonances for both Mo-98 and Mo100. "Staircase" plots were then made that compared the accumulation of observed resonances versus energy to the accumulation of resonances as predicted by the theory of a constant average level spacing. The energy range for the computation of D_0 was [0 keV, 10 keV] for Mo-98 and [0 keV, 26.5 keV] for Mo-100. The maximum energy for Mo-98 was much smaller than the upper range of the resolved resonance region indi-

cated in ENDF/B-VII.1, which is 32 keV. (Chadwick, 2011) The limited range was taken because there were many missing levels above 10 keV for Mo-98. A region is referred to as having 'missing levels' when the assumption of a constant level density breaks down. Details about the level density calculations can be found in the references. (Mughabghab, 2006)

The staircase plot for Mo-98s-wave resonances is given in Fig. 5. The staircase plot for Mo100 s-wave resonances is given in Fig. 6.

As seen in Fig. 5, there appear to be many missing levels for Mo-98s-wave resonances above 10 keV for both the most recent evaluation and the newly fitted resonance parameters. On the other hand, the staircase plot for Mo-100 implies few, if any, missing levels up to 26.5 keV.

Figs. 5 and 6 are complemented by Table 6, which demonstrates the energy dependence of the average level spacings for Mo-98 and Mo-100 for both the newly fitted resonance parameters and those

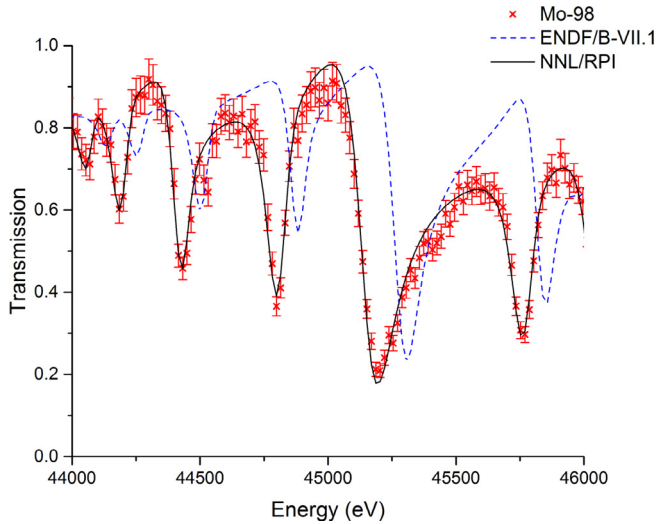


Fig. 3. Transmission and fits for Mo-98 in the range [44 keV, 46 keV]. This Figure demonstrates the improved fit, which included changing s-wave resonances to p-wave resonances at 44789 eV and 45750 eV from ENDF/B-VII.1 to the newly fitted parameters as we as changing a p-wave to an s-wave resonance at 44400 eV. The newly fitted parameters agree much better with the transmission data in this energy range.

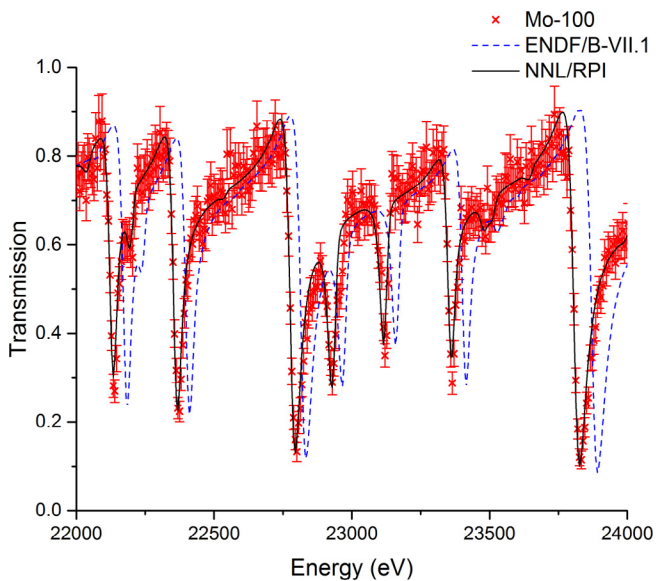


Fig. 4. Transmission and fits for Mo-100 in the range [22 keV, 24 keV]. This plot shows more differences between the newly fitted parameters and those given in the current evaluation. The main difference is a shift in energy, which was verified by a simultaneous measurement of uranium resonances.

found in ENDF/B-VII.1. Also presented in Table 6 are level spacings for Mo-98 and Mo100 from *The Atlas of Neutron Resonances* (Mughabghab, 2006) (*Atlas*).

As seen in Table 6, average level spacing for Mo-98 shows a much greater energy dependence than average level spacing for Mo-100. Computed average level spacings for Mo-98 increase with energy, indicating that fewer levels are seen as energy increases, which echoes the implications of Fig. 5. A greater ‘whole range’ level spacing value for NNL/RPI to ENDF/B-VII.1 is due to the conversion of many s-wave resonance to p-wave resonances in the fitting process, which was discussed in Section 4.1. Computations of average level spacing in the interval [0 keV, 10 keV] resulted in values that were in better agreement with the *Atlas* value for all cases.

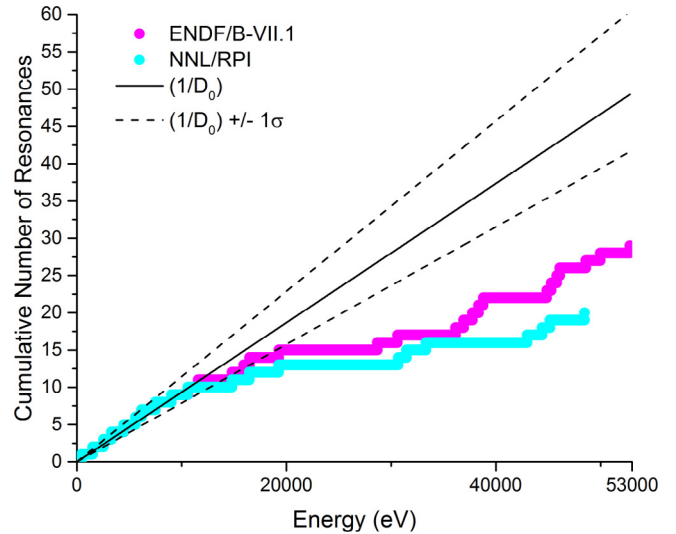


Fig. 5. Staircase plot showing accumulation of s-wave resonances versus energy for Mo-98. The solid plotted line whose slope is $\frac{1}{D_0}$, corresponds to average level spacing D_0 . The dotted lines correspond to average level spacing D_0 plus or minus one standard deviation. For this figure, D_0 was computed for resonances in the range [0 keV, 10 keV].

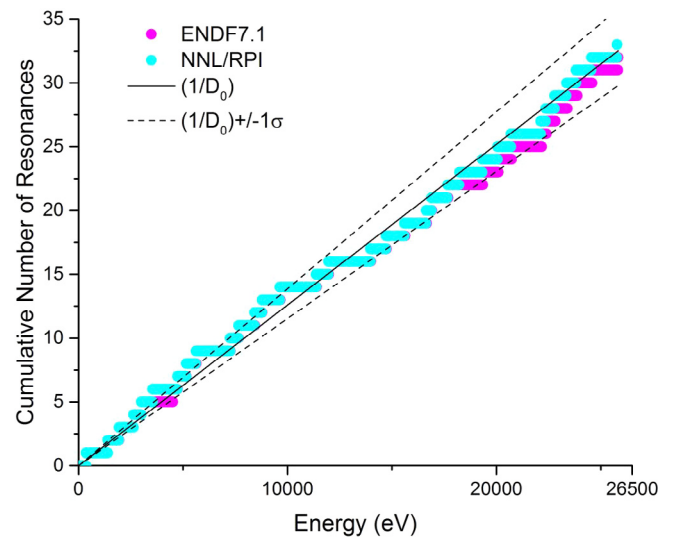


Fig. 6. Staircase plot showing accumulation of s-wave resonances versus energy for Mo-100. The solid plotted line, whose slope is $\frac{1}{D_0}$, corresponds to average level spacing D_0 . The dotted lines correspond to average level spacing D_0 plus or minus one standard deviation. For this figure, D_0 was computed for resonances in the range [0 keV, 26.5 keV].

4.2.2. Strength function

Strength functions for both s- and p-wave resonances for Mo-98 and Mo-100 were computed.

Strength function is defined as

$$S^l = \frac{g\Gamma_n^l}{(2l+1)D_l} \quad (7)$$

where S^l is the strength function for resonances with incident neutrons with l orbital angular momentum quantum number. The quantity $\langle g\Gamma_n^l \rangle$ is the average value of statistical factor g times reduced neutron width Γ_n^l , whose definition is

$$\Gamma_n^l = \left[\frac{1 \text{ eV}}{E} \right]^{\frac{1}{2}} \frac{\Gamma_n}{V_l} \quad (8)$$

Table 6

Average level spacings for s- and p-wave resonances for Mo-98 and Mo-100. In the table, ENDF is ENDF/B-VII.1, NNL/RPI are the newly fitted resonance parameters and 'Atlas Value' entries come from the *Atlas*. In all cases, average level spacing is given in units of eV. All of these values have been calculated by the authors except for the *Atlas* values. While the energy ranges for ENDF and NNL/RPI values are indicated in the table, the energy range for the *Atlas* values is ambiguous.

		Energy Range	ENDF	NNL/RPI	<i>Atlas</i>
Mo-98	s-wave: D_0	[0 keV, 10 keV] [0 keV, 53 keV]	1100 ± 200 1900 ± 200	1100 ± 200 2500 ± 300	970 ± 200
	p-wave: D_1	[0 keV, 10 keV] [0 keV, 53 keV]	290 ± 25 410 ± 20	290 ± 25 390 ± 20	
Mo-100	s-wave: D_0	[0 keV, 10 keV] [0 keV, 26.5 keV]	700 ± 100 820 ± 80	700 ± 100 790 ± 70	617 ± 70
	p-wave: D_1	[0 keV, 10 keV] [0 keV, 26.5 keV]	280 ± 30 290 ± 20	270 ± 30 280 ± 20	

where energy E is given in eV, and penetrability V_l depends upon the value of l . The forms V_l can take are given in Table 7.

For p-wave ($l = 1$) incident neutrons, wave number k in fm^{-1} and nuclear radius R in fm are given by Eqs. (9) and (10), respectively:

$$k = 2.1968 * 10^{-4} \left(\frac{ARWI}{AWRI + 1} \right) \sqrt{E} \quad (9)$$

$$R = 1.23 * AWRI^{1/3} + 0.8 \quad (10)$$

where $AWRI$ is atomic mass to neutron mass ratio and E is in eV.

In the course of this study, an alternative to Eq. (7) was used to determine the strength functions. Plots of cumulative g_l^l vs. energy were made, and best-fit lines based upon $\sum g_l^l$ were determined via least-squares fitting. Once coefficients A , B were obtained for the best-fit line $y = AE + B$, strength function was computed as the slope of the best fit line divided by $2l + 1$. This method was seen as superior to Eq. (7) since it allowed for a graphical view of possible energy dependence of the strength function – these plots are generally linear, and deviation from linearity (e.g., kinks) are examples of energy dependence on the strength function. In addition, this method incorporates energy dependence of the strength function into uncertainty estimates. For more information about the method of strength function estimation, including uncertainty quantification, the reader is referred to [Leinweber et al. \(2018\)](#).

Computed s- and p-wave strength functions are given in Table 8. While resonance parameters are provided from ENDF/B-VII.1 without uncertainties, strength function values from ENDF-sourced resonance parameters are reported with uncertainties. These

uncertainties come from the observed nonlinearity of $\sum g_l^l$ with the plotting method described. The uncertainties in the strength function from the NNL/RPI-sourced resonance parameters come from the uncertainties in the parameters themselves as well as to the observed nonlinearity of $\sum g_l^l$ with the plotting method described.

There are many interesting results presented in Table 8. For Mo-98s-wave resonances, the differences between strength functions from the newly fitted parameters, ENDF parameters, and the *Atlas* value are not statistically significant. However, if strength function computation is extended to the whole range for Mo-98, then there is a marked drop-off in strength function values. While still within error bars of the values computed for resonances up to 10 keV, this decrease suggests missing levels, as seen in the analysis of Section 4.2.1.

For Mo-98p-wave resonances, a similar behavior up to 10 keV is seen – the ENDF value, the NNL/RPI value, and the *Atlas* value are in good agreement. However, when the energy range is extended up to 53 keV, the ENDF and NNL/RPI values diverge, and differences with the *Atlas* value increase. This follows the results of the resonance parameter fits for Mo-98, where particularly at higher energies, rather different resonance parameters from those in the current evaluation were determined from the current measurement.

Table 8 also shows an apparent energy dependence on the Mo-100s-wave strength function, where different values result for the energy ranges [0 keV, 15 keV] and [15 keV, 26.5 keV]. [Weigmann et al. \(1979\)](#) observed this as well. However, for all cases, there is good agreement between the ENDF value for strength function and the NNL/RPI value. For the Mo-100p-wave strength function, there is again good agreement between ENDF and NNL/RPI values. In addition, Mo-100s- and p-wave resonances computed up to 26.5 keV are within error bars of the *Atlas* values.

Table 7
Penetrabilities for incident neutrons, from the *Atlas*.

l	V_l
0	1
1	$\frac{(kR)^2}{1 + (kR)^2}$

Table 8

Strength function values for s- and p-wave resonances for Mo-98 and Mo-100. In the table, ENDF is ENDF/B-VII.1 and NNL/RPI is the newly fitted resonance parameters. Strength function is a dimensionless quantity, but all values given here are reported in units of 10^{-4} . All of these values have been calculated by the authors except for the *Atlas* values.

		Energy Range	ENDF	NNL/RPI	<i>Atlas</i>
Mo-98	s-wave	[0 keV, 10 keV] [0 keV, 53 keV]	0.6 ± 0.3 0.45 ± 0.14	0.7 ± 0.4 0.4 ± 0.2	0.58 ± 0.13
	p-wave	[2.2 keV, 10 keV] [2.2 keV, 53 keV]	5.8 ± 1.2 3.5 ± 1.7	6.2 ± 1.1 7.4 ± 1.0	
Mo-100	s-wave	[0 keV, 10 keV] [15 keV, 26.5 keV] [0 keV, 26.5 keV]	0.5 ± 0.2 1.0 ± 0.2 0.7 ± 0.3	0.4 ± 0.2 0.9 ± 0.2 0.6 ± 0.2	0.8 ± 0.22
	p-wave	[2.7 keV, 26.5 keV]	4.2 ± 0.8	4.2 ± 0.6	

4.2.3. Distribution of neutron widths

Cumulative reduced neutron width distributions were plotted for both the newly fitted resonance parameters and those in ENDF/B-VII.1. The results were plotted along with the distributions

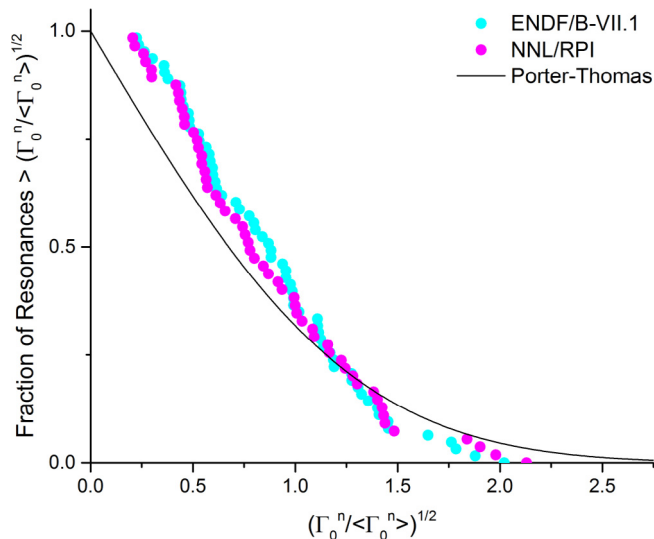


Fig. 7. Cumulative reduced neutron width distributions for Mo-98 and Mo-100s-wave resonances for the new measurement and ENDF/B-VII.1. These resonances were taken from the entire energy range for each isotope – [0 keV, 53 keV] for Mo-98 and [0 keV, 26.5 keV] for Mo100.

predicted by Porter-Thomas theory (Porter and Thomas, 1956), which claims neutron widths are distributed via a χ^2 distribution with one degree of freedom. The distribution of Mo-98 and Mo-100s-wave resonances is plotted in Fig. 7. The plotted points are the s-wave reduced neutron widths Γ_n^0 normalized to the unweighted average value, $\langle \Gamma_n^0 \rangle$, within a spin group, the collection of levels with the same $j\pi$.

For both ENDF/B-VII.1 and the NNL/RPI parameters, there appear to be too many small levels and too few large levels, in comparison to theory. The NNL/RPI parameters offer a small improvement in relation to theory.

5. Conclusions

Transmission measurements for Mo-98 and Mo-100 were performed and analyzed. A 31 m flight path was used to experimentally determine a transmission spectrum in the range [10 eV, 3 keV], and a 100 m flight path was used to experimentally determine transmission spectrum in the range [3 keV, 53 keV] for Mo-98 and [3 keV, 26.5 keV] for Mo-100. Background determination for the experiment was performed via the black notch method, and a fixed black notch was used to normalize the fitted background shape, which was different for the two detectors at 31 m and 100 m.

The results for Mo-98 resulted in a fitted transmission spectrum that was significantly different than the spectrum generated from the resonance parameters of ENDF/B-VII.1. The current resonance parameters themselves vary greatly from those in the current evaluation, particularly at higher energies, as seen in Table 4. Analysis of level statistics shows that a significant number of levels are missing above 10 keV for s-wave resonances.

The results for Mo-100 suggested a refinement of resonance parameters given in the current evaluation. This refinement essentially manifests itself in energy shifts of the data. In addition, a few new resonances were observed and added to Table 5. Level statistics and resonance integrals indicate good agreement with prior results.

Currently, ENDF/B-VII.1 recommends a cutoff for the resolved resonance region for Mo-98 at 32 keV (Chadwick, 2011). However, much of the prior data for resonance parameters for Mo-98 appear

to come from older measurements, such as that of Chrien et al. (1976). The results of the measurement described in this paper appear to be discrepant with these older measurements. It should be noted that the results presented here are derived from measurements with much greater experimental resolution than prior results. The presence of the differences between the current measurement and ENDF/BVII.1, along with the level statistics analysis, which suggests a significant number of missing levels above 10 keV, lead to the conclusion that the resolved resonance region cut-off should be moved below the current 32 keV until the resonance parameters at higher energies are resolved sufficiently.

Acknowledgements

The authors acknowledge with gratitude the support and contributions provided by the RPI LINAC staff (P. Brand, M. Gray, M. Strock, and A. Kerdoun), as well as NNL and RPI researchers (J. Burke, D. Williams, J. Geuther, A. Daskalakis, B. McDermott, E. Blain, and N. Drindak) during the molybdenum measurements.

Appendix A. Validation of the resolution function with U-238

In Section 4.1, it was mentioned that the ‘Oak Ridge Resolution Function’ was used in the fitting of resonance parameters for Mo-98 and Mo-100. To validate the experimental resolution, transmission measurements were also carried out for U-238. These data were then plotted against a fitted transmission profile using resonance parameters for U-238 coming from ENDF/B-VII.1. This plot is given in Fig. A.1. While this plot shows a limited energy range, good agreement between the measured data and the fitted transmission profile was observed up to 20 keV, the entire range of the data supplied from ENDF/B-VII.1. Unlike Figs. 3–4, error bars for the transmission spectrum are suppressed in Fig. A.1 to allow for a clearer demonstration that the measured transmission profile agrees with the profile predicted from the resonance parameters found in ENDF/B-VII.1.

Fig. A.1 demonstrates that the experimental resolution modeled with the Oak Ridge Resolution Function is able to describe the well-known behavior of U-238. This validation means that shifts in resonance energies for Mo-98 and Mo-100 fits, which were observed over the entire range of fitting, demonstrate extensive refinement of Mo resonance energies. Further, the results of the

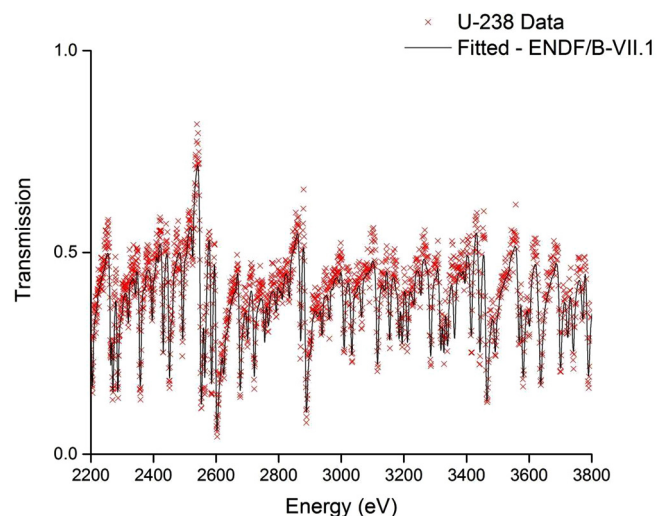


Fig. A.1. A plot of U-238 transmission data plotted against a fit with ENDF/B-VII.1 resonance parameters in the range [2.2 keV, 3.8 keV]. The transmission data in this Figure comes from the 31 m measurements.

U238 measurements can be taken as a validation of the flight path length and t_0 used in transmission data reduction.

Appendix B. . Selection of source data for final resonance parameter set

In Section 4.1, it was mentioned that the source data for the final resonance parameter set came from both the 31 m and 100 m data. While in general, the 31 m data was the source for resonance fit in the energy range 10 eV to 3 keV and the 100 m data was the source for resonance fits in the energy range 3 keV to 53 keV for Mo-98 and 3 keV to 26.5 keV for Mo-100, two resonances were exceptions to this rule. The 1766 eV resonance for Mo-100 was taken from the fit of the 100 m transmission data, and the 3605 eV resonance for Mo-100 was taken from the fit of the 31 m transmission data. The reason for these choices is that the resultant combined fits agreed better with experimental data. Further, these choices had the added benefit that the resultant fits were closer to the resonance parameter values given in ENDF/B-VII.1, so it was viewed that the presented parameters represented a conservative change from previous values. In this appendix, the 31 m transmission spectrum around the 1766 eV and 3605 eV resonances in Mo-100 is plotted alongside the candidate fits originating from data from the 31 m measurements, the 100 m measurements, and a combination of the two. Fig. B.1 shows the transmission spectrum around the 1766 eV resonance, and Fig. B.2 shows the transmission spectrum around the 3605 eV resonance. Unlike Figs. 3–4, error bars for the transmission spectrum are suppressed in Figs. B.1–B.2 to allow for a clearer demonstration that the measured transmission profiles agree well with the combined fit which features the resonance parameters presented in Table 5.

As seen in Fig. B.1, while both fits of the 1766 eV resonance originating from the 31 m data and the 100 m data agree that a shift in energy from the resonance suggested in ENDF/B-VII.1 is appropriate, the fit originating from the 100 m data appear to agree with the measured data better. Therefore, it was used in the combined set of resonance parameters found in Table 5. Fig. B.2 shows that a much improved fit in the energy range [3530 eV, 3620 eV] is obtained if the 3605 eV resonance fit derived from the 31 m transmission data is used. The reason for the improved fit is believed to

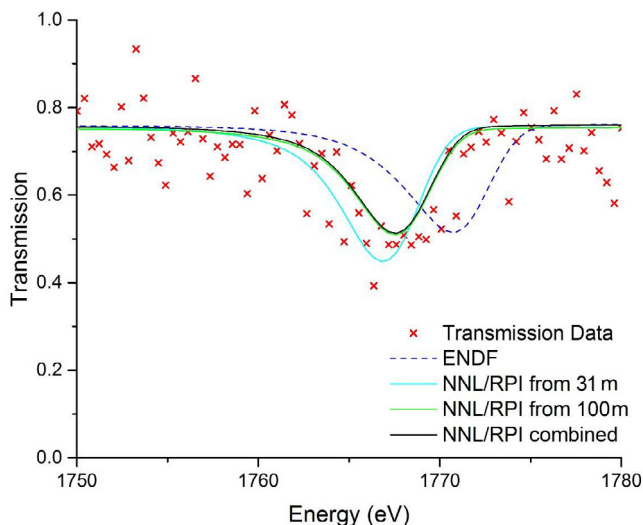


Fig. B.1. The measured transmission spectrum from the 31 m measurements around the 1766 eV resonance plotted alongside fits derived from the 31 m transmission spectrum ('NNL/RPI from 31 m'), from the 100 m transmission spectrum ('NNL/RPI from 100 m'), and from a combination of the 31 m and 100 m transmission spectrum ('NNL/RPI combined').

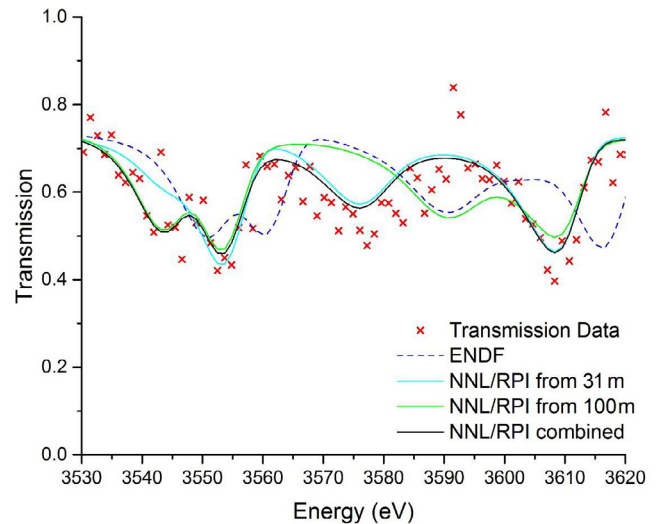


Fig. B.2. The measured transmission spectrum from the 31 m measurements around the 3605 eV resonance plotted alongside fits derived from the 31 m transmission spectrum ('NNL/RPI from 31 m'), from the 100 m transmission spectrum ('NNL/RPI from 100 m'), and from a combination of the 31 m and 100 m transmission spectrum ('NNL/RPI combined') where all resonances come from the 100 m transmission spectrum except for the resonance at 3605 eV, which originates from the 31 m transmission spectrum.

be due to interference with the resonance around 3549 eV. As such, it is appropriate to include the resonance in the combined set of resonance parameters in Table 5.

References

- Bahran, R., 2013. A New High Energy Resolution Neutron Transmission Detector at the Gaertner LINAC Center and Isotopic Molybdenum Total Cross Section Measurements in the keV- Region (Ph.D. thesis). Rensselaer Polytechnic Institute.
- Bahran, R., Barry, D., Block, R., Leinweber, G., Rapp, M., Daskalakis, A., Blain, E., Williams, D., McDermott, B., Leal, L., Danon, Y., 2015. Isotopic molybdenum total neutron cross section in the unresolved resonance region. *Phys. Rev. C* 92 (2), 1–10.
- Barry, D.P., 2003. Neodymium neutron transmission and capture measurements and development of a new transmission detector (Ph.D. thesis). Rensselaer Polytechnic Institute.
- Block, R.C., Bishop, M.C., Barry, D.P., Leinweber, G., Ballad, R.V., Burke, J.A., Rapp, M.J., Danon, Y., Youmans, A., Drindak, N.J., Kim, G.N., Kang, Y.-R., Lee, M.W., Landsberger, S., 2017. Neutron transmission and capture measurements and analysis of Dy from 0.01 to 550 eV. *Prog. Nucl. Energy* 94, 126–132.
- Brown, J.M., Youmans, A., Thompson, N., Danon, Y., Barry, D.P., Leinweber, G., Rapp, M.J., Bahran, R., 2017. Neutron Transmission Measurements and Resonance Analysis of Molybdenum-96. In: *AccApp '17 Proceedings*, July 31st – August 4th 2017, Quebec City, Quebec, Canada.
- Chadwick, M.B. et al., 2011. ENDF/B-VII.1: nuclear data for science and technology: cross sections, covariances, fission product yields and decay data. *Nucl. Data Sheets* 112, 2887.
- Chrien, R.E., Cole, G.W., Slaughter, G.G., Harvey, J.A., 1976. Failure of Bohr's compound nucleus hypothesis for the $^{98}\text{Mo}(n, \gamma)^{99}\text{Mo}$ reaction. *Phys. Rev. C* 13 (2), 578–594.
- Danon, Y., 1993. Design and construction of the RPI enhance thermal neutron target and thermal cross section measurements of rare earth, Ph.D. dissertation, Mech. Aero. Nucl. Eng. Dept. RPI.
- Epping, B.E., Leinweber, G., Barry, D.P., Rapp, M.J., Block, R.C., Donovan, T.J., Danon, Y., Landsberger, S., 2017. Rhenium resonance parameters from neutron capture and transmission measurements in the energy range 0.01 eV to 1 keV. *Prog. Nucl. Energy* 99, 5972.
- Harvey, J.A., Hughes, D.J., Carter, R.S., Pilcher, V.E., 1955. Spacings and neutron widths of nuclear energy levels. *Phys. Rev.* 99 (1), 10–33.
- Larson, N.M., 2008. Updated Users' Guide for SAMMY: Multilevel R-matrix Fits to Neutron Data Using Bayes' Equations. ORNL/TM-9179/R8 ENDF-364/R2. Oak Ridge National Laboratory.
- Leinweber, G., Barry, D.P., Burke, J.A., Drindak, N.J., Danon, Y., Block, R.C., Francis, N. C., Moretti, B.E., 2010. Resonance parameters and uncertainties derived from epithermal neutron capture and transmission measurements of natural molybdenum. *Nucl. Sci. Eng.* 164, 287–303.

- Leinweber, G., Barry, D.P., Burke, J.A., Rapp, M.J., Block, R.C., Danon, Y., Geuther, J.A., Saglime III, F.J., 2014. Europium resonance parameters from neutron capture and transmission measurements in the energy range 0.01–200 eV. *Ann. Nucl. Energy* 69, 74–89.
- Leinweber, G., Barry, D.P., Block, R.C., Burke, J.A., Remley, K.E., Rapp, M.J., Danon, Y., 2018. Cadmium Resonance Parameters from Neutron Capture and Transmission Measurements of Cadmium at the RPI LINAC, DOE Office of Science and Technical Information, OSTI.
- Mason, L., et al., 2011. National Aeronautics Space Administration Report No. NASA/TM-2011217099.
- Moretti, B., 1996. Molybdenum neutron transmission measurements and the development of an enhanced resolution neutron target, Ph.D. dissertation, Mech. Aero. Nucl. Engr. Dept., RPI, Troy, NY.
- Mughabghab, S.F., 2006. *Atlas of Neutron Resonances: Resonance Parameters and Thermal Cross Sections Z = 1–100*. Elsevier, Amsterdam, Netherlands.
- Phillips, A.M., Mickum, G.S., Burkes, D.E., 2010. Idaho National Laboratory Report No. INL/EXT-10-19373.
- Porter, C.E., Thomas, R.G., 1956. Fluctuations of nuclear reaction widths. *Phys. Rev.* 104, 483.
- Rest, J., et al., 2009. Argonne National Laboratory Report No. ANL-09/31.
- Shwe, J., Coté, R.E., 1969. Neutron resonances of mo isotopes. *Phys. Rev.* 179 (4), 1148–1153.
- Wang, T.F. et al., 2008. Measurement of the total neutron cross-section and resonance parameters of molybdenum using pulsed neutrons generated by an electron linac. *Nucl. Instrum. Methods Phys. Res. B* 266, 561–569.
- Weigmann, H., Raman, S., Harvey, J.A., Macklin, R.L., Slaughter, G.G., 1979. Neutron resonances in 100Mo and valence neutron capture. *Phys. Rev. C* 20 (1), 115–127.
- Wynchank, S., Garg, J.B., Havens Jr., W.W., Rainwater, J., 1968. Neutron resonance spectroscopy. VI. Mo, Sb, Te, and Pr. *Phys. Rev.* 166 (4), 1234–1259.